Astron. Astrophys. 336, 242–250 (1998)

ASTRONOMY
AND
ASTROPHYSICS

The nature of isolated T Tauri stars⋆

Wilhelm Hoff, Thomas Henning, and Werner Pfau

Astrophysikalisches Institut und Universitäts-Sternwarte Jena, Schillergässchen 2, D-07745 Jena, Germany

Received 4 July 1997 / Accepted 19 May 1998

Abstract. We present the results of a search for young stellar objects around the two isolated T Tauri stars (TTSs) TW Hya and CoD$-29°8887$. From the spectroscopic properties of these two objects, it is obvious that they are T Tauri stars, although they are not associated with a star-forming region as it is the case for most of the known TTSs. Especially TW Hya is the only classical TTS that is not located in a dark cloud with star formation activity. The same is true for the weak-line T Tauri star CoD$-29°8887$.

We searched for pre-main sequence stars using ROSAT PSPC observations pointing at our two main targets. With a sophisticated search strategy we could identify 107 X-ray sources in our fields. For the 37 stellar-like optical counterparts we did spectroscopic follow-up observations. These show that within the viewing field of ROSAT there are no other X-ray emitting young stellar objects around TW Hya and CoD$-29°8887$.

For the isolated TTSs TW Hya and HD 98800 Hipparcos parallax measurements are available locating them at distances of 56 and 46pc, respectively. This means that they are the closest TTSs with circumstellar dusty disks known today. The space velocities of these two objects are 3–5km/sec. From their position in the HR diagram, we obtained an age of about 10^7 years. Hence, we conclude that these two objects travelled not far away from their original birthplace and their parental molecular cloud dispersed meanwhile. This is the solution why these T Tauri stars appear to be isolated.

Key words: stars: formation – stars: pre-main sequence – stars: individual: TW Hya – stars: individual: CoD$-29°8887$ – stars: individual: HD 98800 – X-rays: stars

1. Introduction

The spatial distribution of pre-main sequence (PMS) stars is an important clue to understand the evolution of molecular clouds and the process of star formation. Therefore, many surveys have been carried out to search for T Tauri stars (TTSs) located in molecular clouds. In addition, ROSAT revealed a population of weak-line TTSs up to 10pc away from regions like the Taurus-Auriga complex or the system of Chamaeleon dark clouds where low-mass stars are formed, c.f., Neuhäuser (1997) for a recent review and references therein. Furthermore, there are a few TTSs which reveal all the characteristics of low-mass PMS stars, but are more or less isolated from any known star-forming region. They are usually called *isolated* TTSs. The phenomenon of isolated young stellar objects (YSOs) is already well-known for the Herbig Ae/Be stars (Grinin et al. 1991, Thé et al. 1994).

A prototype of isolated TTSs is TW Hya. Hoffmeister (1943) noticed the 'short-period' variability of TW Hya, but he was not able to determine the exact type of variability. In his Hα survey, Henize (1976) found TW Hya to possess a very strong Hα emission line. With spectra based on 33 Å/mm plates, Herbig (1978) found additional emission lines which underline the T Tauri character of TW Hya.

Later on, CoD$-29°8887$ and Hen(3)600 were classified as isolated TTSs (de la Reza et al. 1989). Using the IRAS point source catalogue, Gregorio-Hetem et al. (1992) added CoD$-33°7795$ as the fourth member to this remarkable group of young stellar objects. From recent investigations by Soderblom et al. (1996) combined with the Hipparcos parallax measurements, one knows that the multiple T Tauri star system HD 98800 has to be added to this group. All these objects are located within a field of 10×10 square degrees near the position (l,b)=(278°, 23°). This is far away from any known star-forming region. The nearest dark cloud, namely Sa 122 (Sandqvist 1977), is located at (l,b)=(280°, 10°), 13° apart from the position of the objects.

Classical T Tauri stars (CTTS) are normally associated with molecular clouds with ongoing star formation. They show strong Hα emission, forbidden emission lines, strong LiI $\lambda6708$ absorption, and often ultraviolet and infrared excesses in their spectral energy distributions. As Rucinski & Krautter (1983) had already shown, TW Hya shares all the properties of a CTTS, but is not associated with a dark cloud. It is remarkable that it is nevertheless a strong infrared and submillimetre source (Weintraub et al. 1989, see also Fig. 1) and shows relatively narrow molecular line profiles (Zuckerman et al. 1995) indicating the presence of a compact dust-gas envelope and/or disk at the position of TW Hya. Circumstellar dust radiation was

Send offprint requests to: Wilhelm Hoff, (hoff@astro.uni-jena.de)

⋆ Based on observations obtained at the European Southern Observatory, La Silla, Chile

also found in case of HD 98800 (Zuckerman & Becklin 1993, Zuckerman et al. 1995). Another TTS, namely CoD$-29°8887$, is located 4° north of TW Hya. It is classified as a weak-line T Tauri star (WTTS). WTTSs neither show any excess at UV wavelengths nor forbidden emission lines. Their Hα emission is weaker (EW(Hα) < 10Å) than in case of a CTTS. The lithium line strength is of the same order, however, and proves that these objects are PMS stars.

A possible explanation of the presence of TTSs far away from molecular clouds and especially of the phenomenon of isolated TTSs is the ejection of these objects from their original birthplaces (Sterzik & Durisen 1995). Some stars may indeed have escaped from their parent clouds because of large velocity dispersions within the stellar groups, but these objects very probably do not form the majority of the TTSs detected by ROSAT outside the boundaries of the molecular clouds (see, e.g., Palla & Galli 1997). Another explanation for their great distances to any dark cloud might be that they have formed from small molecular clouds which later were dispersed (Feigelson 1996). In this case, we would expect to find further YSOs close to TW Hya and CoD$-29°8887$ if multiple star formation takes place in such cloudlets. Such a mode of star formation is indeed confirmed in Bok globules with star formation activity (Launhardt & Henning 1997). To distinguish between these scenarios, we performed ROSAT PSPC observations pointing at TW Hya and CoD$-29°8887$. The goal was to detect additional YSOs from their X-ray emission produced by chromospheric and coronal activity. Strong X-ray emission is typical for PMS stars and may exceed the emission from main-sequence stars of the same spectral type by a factor of 10^3 (e.g. Neuhäuser et al. 1995).

Sect. 2 summarises the details of the X-ray observations. For stellar-like optical counterparts coinciding with the X-ray sources detected within our fields we got spectroscopic follow-up observations in order to decide on their nature as TTSs. In Sect. 3 the TTS detection algorithms are described and the results are presented. In Sect. 4 we discuss the results including a more detailed analysis of the X-ray data and the distances of the objects. Sect. 5 gives our conclusions on the formation scenario of isolated TTSs.

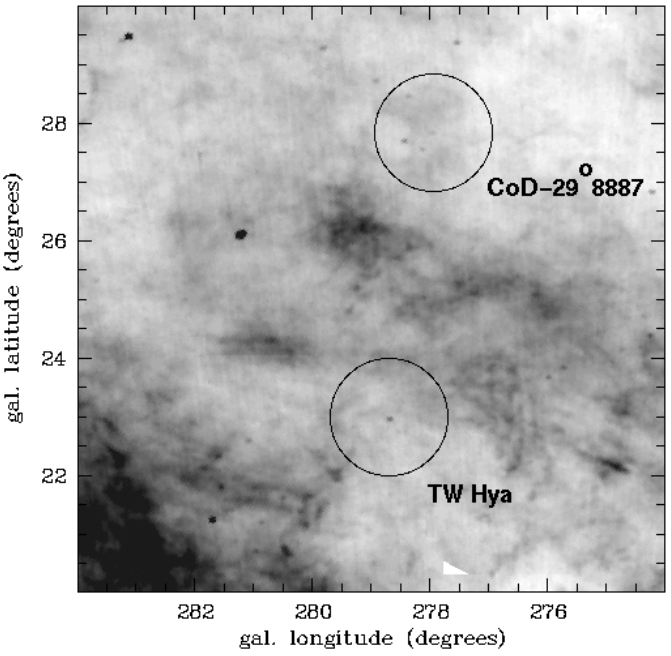

Fig. 1. IRAS 100-μm map with overlayed viewing fields of the ROSAT pointings

2. Observations

2.1. X-ray observations

We obtained two X-ray observations using the position-sensitive proportional counter (PSPC(B)) camera onboard of ROSAT which operates in the soft X-ray energy range between 0.1 and 2.4keV. This range is very suitable to search for low-mass YSOs, as it turned out from surveys carried out with the Einstein Observatory (Feigelson 1987, Walter et al. 1988). A detailed description of the ROSAT telescope and the PSPC are given by Trümper et al. (1991). The ROSAT pointings were done on December 12 and 17, 1991 for TW Hya and CoD$-29°8887$, respectively. The total effective exposure times were about 6.7 and 6.5ksec, respectively, more than ten times deeper than the ROSAT All-Sky Survey (RASS) at that position. From the X-ray count rates measured for the weakest sources, $s = 2 \cdot 10^{-3}$/s, together with an energy conversion factor of $ECF = 10^{-11}$erg/cm^2 (Neuhäuser et al. 1995) typical for TTSs, we get a detection limit of $f_{\rm X} = 2 \cdot 10^{-14}$erg/(cm^{2}s) for our observations. For a given 3σ lower limit of $L_{\rm X} = 10^{29}$erg/s for the X-ray luminosity of a TTS (Pfau et al. 1998), we expect completeness in our detection of TTSs out to a distance of 210pc. Our targets are located at a high galactic latitude of b = 25°. Assuming a typical galactic scale height for YSOs of 65pc, we statistically expect only five percent of the TTSs to be farther away than 215pc. This is comparable with our limit of completeness and we should have found all YSOs within our fields of view.

A 100-μm IRAS map of the region around TW Hya and CoD$-29°8887$ is shown in Fig. 1. The PSPC fields of view and the positions of these isolated TTSs are overlayed on this map.

2.2. Optical observations

The optical counterparts of the X-ray sources were selected by inspection of finding charts taken from the Digitized Sky Survey (DSS). We overlayed the finding charts with the contour map of an X-ray image binned to the pixel size of the DSS and convolved it with the theoretical point-spread function at the given detector plane position. From these finding charts, we were able to select well-defined optical counterparts for spectroscopic follow-up observations. Our strategy was to include all point-like sources from the DSS finding charts falling within the 2σ X-ray contour line and having a magnitude $m_{\rm V}$ brighter than 16mag.

Only for a few cases the identification of a stellar-like optical counterpart was obvious, while in most cases two or more objects are located at the image position of the X-ray source, or

Table 1. Set-up of the B&C spectrograph at the 1.52-m ESO telescope. The CCD detector FORD 2048L ♯24 (2048×2048 15μm-sized pixels) was used.

Period	Grating (Order)	Central wavelength	Resolution
1993, Mar. 13 to 19	♯ 26 (1 st)	450 nm	0.20 nm
		650 nm	0.21 nm
1996, Feb. 20 to 27	♯ 5 (1 st)	590 nm	0.30 nm

there was no bright source at all. In the latter case, we expect most of these sources to be extragalactic.

Spectroscopic follow-up observations were carried out with the B&C spectrograph of the ESO 1.52-m telescope on La Silla, Chile, during two observing runs. The instrumental set-up is given in Table 1. This table also includes the spectral resolution which was derived by measuring the full width at half maximum of several lines of the comparison spectra. The Reduction of the spectra was done using the MIDAS software.

3. Results

3.1. Detection of X-ray sources

Our source detection algorithm utilises procedures that are defined within the MIDAS application Extended Scientific Analysis System (EXSAS). In a first step we have to create images for the source detection procedures. The events are selected from the photon event table for five different energy bands and binned to images with a pixel size of 15 arcsec. There are five different energy ranges: "broad" (0.2–2.2keV), "soft" (0.2–0.5keV), "hard" (0.6–1.9keV), "hard1" (0.6–0.9keV), and "hard2" (0.9–1.9keV).

Within each energy band image, we searched for X-ray sources using a sliding window source detection technique. The sliding window is defined as a 5×5 pixel area. In a first run the inner area of 3×3 pixels is compared to the surrounding 16 pixels ring providing a likelihood for a point source at the window centre, which is calculated from a binomial and χ^2 probability table. If the likelihood of existence of the source falls above the 4σ-confidence level, it is added to the source list of the corresponding energy band. These five lists are used to generate smoothed background images by cutting out the detected sources and performing a bicubic spline fit to the remaining images. In a second run the sliding window procedure uses only the inner pixel area and the background information just derived. The detected sources are written to a second group of lists. For each energy band the two lists are merged into one table of source positions. Two sources are called identical, if the distance between them is smaller than two times the size of the inner sliding window or smaller than the point spread function of the instrument.

The third procedure uses a maximum likelihood technique that works on the photon event data and the smoothed background images. It compares the observed photon distribution above the background level with the spatial distribution of a theoretical point-spread function. This results in a likelihood that both distributions are identical. The likelihood is defined as $ML = -\ln(1-P)$, where P is given as the source existence probability, and is maximised by varying the source extent and position. At this point, all sources with a maximum likelihood $ML > 0$ are merged into one list of final source positions.

Since a source is not necessarily detected within all five energy bands, we have to apply an upper limit maximum likelihood procedure to derive the X-ray properties at a source position within each energy band. At the end, we merged the results into a final list containing the source positions and X-ray properties depending on the maximum likelihood for source existence. This threshold is set to $ML = 6$ for the first four bands corresponding to a confidence level of source existence of 3.5σ. For the "hard2" energy band it is set to $ML = 10$ because of the poor background statistics within this band.

The resulting lists of detected X-ray sources around our two main targets are given in Tables 2 and 3. Column (1) gives the source numbers of the detected X-ray sources. The columns (2) and (3) contain the source coordinates and column (4) the maximum likelihood for the existence of a source at the given position. The count rates (column 5) are corrected for vignetting of the telescope and dead times of the detector. Columns (6) and (7) provide spectral information about the X-ray sources using the hardness ratios $HR1$ and $HR2$ defined as

$$HR1 = \frac{hard - soft}{hard + soft}, \quad HR2 = \frac{hard2 - hard1}{hard2 + hard1}. \qquad (1)$$

The variables $soft$, $hard$, $hard1$, and $hard2$ represent the number counts within the corresponding energy bands.

We detected a total number of 107 X-ray sources around the two isolated TTSs. All these X-ray sources have been checked for counterparts within the NASA Extragalactic Database (NED) and SIMBAD, and have been supplemented by information from finding charts taken from the Digitized Sky Survey (DSS). Cross-identifications with HST GSC sources are also given. For 41 X-ray sources we found counterparts that are compiled in Table 4. The column 'object type' describes the appearance of an optical counterpart in the DSS. The entry 'distance' in Table 4 gives the separation between its optical and the X-ray position. In the case of 7 X-ray sources we found more than one optical candidate in the GSC or the DSS.

By inspecting the finding charts we found that in most cases the objects with $m_{\rm V}$ weaker than 16mag are clearly associated with an extragalactic object. Thus, the fraction of stellar objects fainter than this limiting magnitude in the X-ray data base should be very low. We additionally identified a new cluster of galaxies as the optical counterpart of the X-ray source TW HyaX01. Five X-ray sources are very probably associated with clusters of galaxies given as 'cluster (cand.)' in Table 4. Altogether 37 stellar-like optical candidates with $m_{\rm V}$ brighter than 16mag remained for our spectroscopic follow-up observations.

Table 2. Sources around TW Hydrae

Name	α_{2000}			δ_{2000}			ML	count rate	HR 1	HR 2
TW HyaX	(h)	(m)	(s)	(°)	(′)	(″)		(cts/ksec)		
1	10	58	08.22	-34	42	23.6	150.5	42.2 ± 5.3	0.86 ± 0.07	0.27 ± 0.08
2	10	59	44.95	-34	46	18.3	16.6	7.1 ± 2.0	0.49 ± 0.09	-0.00 ± 0.14
3	10	59	52.75	-34	45	53.3	28.3	10.5 ± 2.2	0.62 ± 0.12	0.11 ± 0.14
4	11	00	02.14	-35	06	50.4	29.4	17.7 ± 2.9	-0.70 ± 0.08	-0.01 ± 0.37
5	11	00	26.93	-34	56	58.6	10.0	2.0 ± 0.6	1.00 ± 0.52	-0.01 ± 0.16
6	11	00	30.34	-34	35	06.7	12.2	4.8 ± 0.9	1.00 ± 0.37	0.11 ± 0.14
7	11	00	38.80	-34	46	13.6	15.3	7.2 ± 1.5	-0.01 ± 0.17	-0.51 ± 0.13
8	11	00	50.00	-34	43	25.5	76.9	10.3 ± 1.5	0.65 ± 0.09	0.13 ± 0.15
9	11	00	51.41	-35	33	07.0	9.9	6.0 ± 3.0	1.00 ± 0.56	-0.77 ± 0.23
10	11	01	02.12	-34	32	00.8	7.1	2.0 ± 0.5	0.59 ± 0.35	-0.34 ± 0.18
11	11	01	03.00	-34	48	48.3	11.0	0.7 ± 0.3	1.00 ± 0.77	1.00 ± 0.37
12	11	01	06.73	-34	53	18.9	10.2	2.1 ± 0.5	0.28 ± 0.40	1.00 ± 0.35
13	11	01	07.01	-34	41	18.9	21.2	4.6 ± 1.0	-0.01 ± 0.21	-0.09 ± 0.17
14	11	01	17.31	-34	51	55.6	7.5	0.9 ± 0.3	1.00 ± 0.59	-0.11 ± 0.18
15	11	01	18.56	-34	53	09.7	54.5	5.4 ± 1.1	0.79 ± 0.12	0.09 ± 0.18
16	11	01	25.29	-34	40	41.8	57.1	5.2 ± 1.0	0.70 ± 0.16	0.24 ± 0.20
17	11	01	25.46	-34	32	55.3	10.2	1.8 ± 0.4	0.38 ± 0.35	0.39 ± 0.25
18	11	01	31.22	-34	10	56.3	11.8	4.8 ± 1.1	0.24 ± 0.21	-0.37 ± 0.19
19	11	01	32.42	-34	42	35.9	24.8	3.9 ± 1.0	0.15 ± 0.22	0.42 ± 0.18
20	11	01	33.04	-34	40	33.4	8.0	0.9 ± 0.3	1.00 ± 0.70	-0.46 ± 0.17
21	11	01	37.37	-34	04	25.9	17.0	1.4 ± 1.9	1.00 ± 0.22	0.56 ± 0.15
22	11	01	37.85	-34	16	40.9	17.4	3.4 ± 0.8	1.00 ± 0.29	0.63 ± 0.11
23	11	01	42.98	-34	52	57.4	7.2	1.0 ± 0.3	1.00 ± 0.73	0.27 ± 0.19
24	11	01	44.23	-35	02	13.9	13.1	2.8 ± 0.6	0.71 ± 0.30	-0.01 ± 0.23
25	11	01	46.76	-34	57	17.0	43.1	7.6 ± 1.4	0.24 ± 0.14	-0.18 ± 0.20
26	11	01	48.26	-34	54	56.5	8.5	1.6 ± 0.4	1.00 ± 0.98	0.12 ± 0.18
27	11	01	48.77	-34	34	35.5	18.3	2.2 ± 0.7	0.89 ± 0.45	0.13 ± 0.25
28	11	01	50.35	-34	37	19.5	20.7	2.3 ± 0.7	0.78 ± 0.32	-0.11 ± 0.26
29	11	01	51.88	-34	47	52.0	6.9	1.1 ± 0.3	0.79 ± 0.64	-0.39 ± 0.18
30	11	01	52.01	-34	42	23.0	9650.6	308.1 ± 6.8	0.58 ± 0.01	-0.12 ± 0.02
31	11	01	52.05	-34	43	56.0	13.8	3.6 ± 1.0	-0.73 ± 0.09	-0.47 ± 0.21
32	11	01	55.60	-34	40	14.0	22.6	2.7 ± 0.8	0.79 ± 0.42	0.38 ± 0.18
33	11	02	01.57	-34	23	42.4	257.0	21.9 ± 2.1	0.63 ± 0.08	0.31 ± 0.09
34	11	02	06.49	-34	52	02.4	13.2	2.3 ± 0.5	0.78 ± 0.58	-0.14 ± 0.25
35	11	02	09.67	-34	42	49.4	7.8	1.1 ± 0.3	1.00 ± 0.95	0.04 ± 0.21
36	11	02	10.33	-33	59	52.9	24.4	1.3 ± 2.6	1.00 ± 0.11	0.11 ± 0.14
37	11	02	17.31	-34	30	43.8	23.2	2.7 ± 0.8	0.69 ± 0.26	0.23 ± 0.27
38	11	02	19.07	-35	04	56.3	11.6	12.4 ± 1.8	0.61 ± 0.12	-0.67 ± 0.09
39	11	02	21.58	-34	12	38.3	6.8	2.0 ± 1.1	0.48 ± 0.48	-0.18 ± 0.20
40	11	02	24.33	-35	11	30.2	18.6	0.9 ± 0.7	-0.62 ± 0.10	-0.05 ± 0.18
41	11	02	25.22	-35	03	52.2	15.6	4.0 ± 1.2	1.00 ± 0.25	0.11 ± 0.21
42	11	02	28.85	-34	32	00.6	8.6	1.5 ± 0.4	1.00 ± 0.68	-0.06 ± 0.19
43	11	02	30.81	-34	38	42.1	18.8	3.1 ± 0.8	0.70 ± 0.29	-0.53 ± 0.16
44	11	02	35.77	-34	46	12.5	10.1	1.2 ± 0.3	1.00 ± 0.68	-0.31 ± 0.17
45	11	02	36.11	-34	42	44.0	16.5	2.5 ± 0.8	0.45 ± 0.26	0.01 ± 0.27
46	11	02	43.52	-35	21	41.3	39.9	64.1 ± 4.8	1.00 ± 0.31	-0.62 ± 0.15
47	11	02	43.44	-34	46	05.8	20.9	2.6 ± 0.8	0.79 ± 0.52	0.49 ± 0.18
48	11	02	50.15	-34	43	37.1	15.4	2.2 ± 0.4	0.73 ± 0.20	-0.04 ± 0.17
49	11	02	53.09	-34	48	35.5	6.9	1.6 ± 0.4	0.26 ± 0.41	0.16 ± 0.20
50	11	03	01.17	-34	42	53.8	12.0	1.8 ± 0.4	0.91 ± 0.53	0.14 ± 0.17
51	11	03	02.95	-34	48	15.2	10.1	1.8 ± 0.5	-0.01 ± 0.22	1.00 ± 0.16
52	11	03	04.10	-34	40	31.2	10.3	2.4 ± 0.5	0.63 ± 0.25	-0.32 ± 0.15
53	11	03	08.15	-34	43	07.0	7.7	2.6 ± 0.7	1.00 ± 0.35	0.55 ± 0.13
54	11	03	19.08	-34	53	54.6	12.4	2.7 ± 0.6	-0.05 ± 0.20	0.28 ± 0.23
55	11	03	24.62	-34	43	14.8	7.0	0.0 ± 0.6	0.69 ± 0.75	0.53 ± 0.16
56	11	03	33.11	-34	56	11.9	26.6	10.6 ± 1.9	-0.35 ± 0.15	-0.41 ± 0.17
57	11	03	45.18	-34	18	07.7	9.7	4.1 ± 1.1	-1.00 ± 0.13	0.00 ± 0.00
58	11	04	02.55	-34	49	56.2	6.6	0.0 ± 1.2	1.00 ± 0.33	-0.46 ± 0.16

Table 3. Sources around CoD−29°8887

Name	α_{2000}			δ_{2000}			ML	count rate	HR 1	HR 2
CoD-29°8887X	(h)	(m)	(s)	(°)	(′)	(″)		(cts/ksec)		
1	11	05	56.27	-30	21	59.9	19.4	1.0 ± 1.3	1.00 ± 0.11	0.09 ± 0.18
2	11	07	08.93	-29	50	51.4	11.3	0.6 ± 1.2	1.00 ± 0.24	0.18 ± 0.21
3	11	07	27.48	-30	28	56.9	42.7	20.0 ± 3.0	0.63 ± 0.14	0.08 ± 0.15
4	11	07	29.53	-30	06	26.5	46.5	2.0 ± 0.6	0.70 ± 0.33	0.38 ± 0.18
5	11	07	30.19	-29	23	20.0	16.6	90.4 ± 6.1	0.00 ± 0.05	0.82 ± 0.23
6	11	07	30.86	-29	38	18.5	7.5	2.7 ± 1.0	1.00 ± 0.87	0.05 ± 0.18
7	11	07	50.21	-30	04	27.4	18.7	5.2 ± 1.2	-0.09 ± 0.20	0.40 ± 0.22
8	11	07	54.87	-30	10	21.1	22.2	5.2 ± 1.3	-1.00 ± 0.09	-1.00 ± 3.88
9	11	08	03.24	-30	00	23.8	9.4	1.9 ± 0.4	0.25 ± 0.37	0.49 ± 0.20
10	11	08	21.73	-29	44	56.9	7.0	0.7 ± 0.4	1.00 ± 0.69	0.20 ± 0.18
11	11	08	22.12	-30	07	43.4	9.9	2.2 ± 0.5	0.09 ± 0.35	0.53 ± 0.21
12	11	08	25.62	-30	12	52.5	8.8	1.2 ± 0.4	1.00 ± 0.68	-0.14 ± 0.18
13	11	08	27.18	-30	01	00.5	12.6	1.9 ± 0.4	0.07 ± 0.33	-0.08 ± 0.19
14	11	08	29.54	-30	09	22.5	8.3	1.3 ± 0.3	0.69 ± 0.53	0.21 ± 0.19
15	11	08	34.53	-30	07	43.1	113.0	11.8 ± 1.5	-0.19 ± 0.12	-0.33 ± 0.17
16	11	08	35.54	-30	11	37.6	30.4	5.1 ± 1.2	0.69 ± 0.19	0.19 ± 0.16
17	11	08	42.13	-30	06	31.8	23.6	3.9 ± 0.9	0.10 ± 0.19	-0.01 ± 0.30
18	11	08	59.68	-29	37	42.9	18.8	5.0 ± 1.4	0.69 ± 0.24	0.23 ± 0.17
19	11	09	08.01	-30	20	27.5	10.9	4.1 ± 1.2	-0.21 ± 0.20	-0.37 ± 0.23
20	11	09	09.72	-30	02	53.5	10.5	2.3 ± 0.5	-1.00 ± 0.14	0.00 ± 0.00
21	11	09	10.25	-30	13	13.5	8.5	1.8 ± 0.5	0.24 ± 0.50	-0.33 ± 0.18
22	11	09	13.25	-30	24	48.0	7.0	1.6 ± 0.7	1.00 ± 0.73	0.13 ± 0.23
23	11	09	14.05	-30	01	37.0	4729.5	177.3 ± 5.2	0.10 ± 0.02	-0.07 ± 0.03
24	11	09	15.71	-30	03	05.5	92.9	12.3 ± 1.5	-0.79 ± 0.07	0.63 ± 0.16
25	11	09	16.58	-29	50	07.0	20.6	2.7 ± 0.9	0.72 ± 0.17	-0.15 ± 0.26
26	11	09	19.09	-30	00	47.0	45.3	6.2 ± 1.2	-0.97 ± 0.03	-1.00 ± 3.71
27	11	09	24.24	-30	14	33.4	11.2	1.7 ± 0.4	1.00 ± 0.84	0.15 ± 0.19
28	11	09	28.19	-29	37	46.4	23.0	5.4 ± 1.6	0.54 ± 0.20	0.05 ± 0.21
29	11	09	34.45	-30	09	26.3	65.0	6.1 ± 1.1	0.42 ± 0.12	0.34 ± 0.19
30	11	09	36.31	-30	12	19.8	12.9	3.4 ± 1.0	0.29 ± 0.30	-0.07 ± 0.17
31	11	09	38.53	-30	01	00.3	9.3	1.8 ± 0.4	0.30 ± 0.36	0.34 ± 0.28
32	11	09	39.18	-29	33	24.8	12.8	4.0 ± 1.2	1.00 ± 0.16	0.10 ± 0.19
33	11	09	39.56	-30	06	18.3	8.1	2.1 ± 0.8	-0.09 ± 0.20	-0.38 ± 0.20
34	11	09	40.43	-30	02	27.3	7.5	1.3 ± 0.3	0.36 ± 0.38	-0.45 ± 0.19
35	11	09	40.62	-29	47	09.3	8.1	1.4 ± 0.5	1.00 ± 0.56	-0.01 ± 0.18
36	11	09	40.72	-29	59	17.8	23.1	2.6 ± 0.8	0.76 ± 0.27	-0.08 ± 0.31
37	11	09	49.06	-30	04	23.1	10.6	0.7 ± 0.3	1.00 ± 0.74	1.00 ± 0.39
38	11	09	49.13	-30	08	35.6	53.3	3.7 ± 0.9	1.00 ± 0.12	0.27 ± 0.19
39	11	09	50.85	-29	55	21.1	7.5	1.7 ± 0.4	0.46 ± 0.44	-0.47 ± 0.17
40	11	09	56.62	-29	49	09.0	29.7	3.6 ± 1.0	1.00 ± 0.23	0.06 ± 0.22
41	11	10	02.10	-30	10	19.9	10.1	1.2 ± 0.3	1.00 ± 0.64	-0.09 ± 0.19
42	11	10	05.37	-29	57	03.3	64.2	9.6 ± 1.5	0.82 ± 0.06	0.21 ± 0.13
43	11	10	13.00	-30	13	34.6	9.7	1.2 ± 0.4	1.00 ± 0.61	-0.63 ± 0.27
44	11	10	30.68	-30	17	28.5	8.8	1.1 ± 0.8	1.00 ± 0.35	-0.42 ± 0.12
45	11	10	32.90	-30	27	00.9	82.2	17.5 ± 2.7	0.56 ± 0.08	0.13 ± 0.12
46	11	10	44.67	-29	48	52.4	22.4	8.9 ± 1.7	0.14 ± 0.15	0.39 ± 0.14
47	11	10	52.94	-30	11	39.1	44.4	7.5 ± 1.7	0.84 ± 0.18	0.32 ± 0.16
48	11	11	10.21	-30	09	33.2	295.5	43.7 ± 3.5	1.00 ± 0.03	0.23 ± 0.06
49	11	11	38.79	-30	07	06.9	25.6	6.2 ± 1.2	1.00 ± 0.29	0.02 ± 0.20

3.2. Optical identifications

To identify an object from the list of 37 stellar-like sources of Table 4 as a TTS candidate, we adopted the following criteria:

– The presence of the LiI $\lambda 6708$ absorption line. Lithium is easily depleted by thermonuclear reactions with protons or ^{3}He nuclei at a temperature of more than $2.5 \cdot 10^6$K. Since

Table 4. Optical counterparts of X-ray sources

X-ray source	object name / identifier	object type	dist. ($''$)	m_V (mag)	spectral type	EW(LiI) (Å)	EW(Hα) (Å)	remark [a]
TW HyaX01		cluster [b]	-	-				4
TW HyaX04	CoD$-34°7135$	stellar-like	32	12.2	K6e	0.03 ± 0.05	-0.17	1, 3
TW HyaX06	GSC 7208.1002	stellar-like	33	13.6	K0f	-	0.50	3
TW HyaX08		cluster [b] (cand.)	-	-				4
TW HyaX09	SAO 202002	stellar-like	30	8.8	F6	0.15 ± 0.07	4.25	1, 3
TW HyaX10	GSC 7208.0732	stellar-like	30	11.7	F6	0.08 ± 0.05	4.88	3
	GSC 7208.0970	stellar-like	30	13.1	G8	-	2.97	3
	GSC 7208.1098	stellar-like	37	13.4	G5	-	3.03	3
TW HyaX15	GSC 7208.0007	stellar-like	49	14.6	G7	0.05 ± 0.05	2.63	3
TW HyaX16	GSC 7208.1081	stellar-like	38	14.8	G9	-	1.66	3
TW HyaX17	GSC 7208.1254	stellar-like	10	13.9	F5	-	5.48	3
TW HyaX18	GSC 7208.0206	stellar-like	59	13.1	F7	-	4.15	3
TW HyaX23		stellar-like	9	15.5	K0	-	1.55	4
TW HyaX25		stellar-like	10	15.5	K3e	-	-1.05	4
TW HyaX27	GSC 7208.0992A	stellar-like	42	14.9	F5	-	5.05	3
	GSC 7208.0992B	stellar-like	39	15.5	F7	0.07 ± 0.05	4.60	4
TW HyaX28	GSC 7208.0123	stellar-like	46	12.5	G0	0.05 ± 0.05	3.85	3
TW HyaX30	**TW Hya**	stellar-like	7	12.1	K6	0.37 ± 0.09	-225	1, 3
TW HyaX33	TW HyaX33A	stellar-like	6	16.0	K0	-	1.50	4
	TW HyaX33B	stellar-like	15	15.5	F5	-	5.00	4
TW HyaX37	GSC 7208.1270	stellar-like	100	11.8	G7	-	1.75	3
TW HyaX39		stellar-like	9	15.5	K2e	-	-0.35	4
TW HyaX43	GSC 7208.0445	stellar-like	50	12.6	K1	-	1.75	3
	GSC 7208.0559	stellar-like	58	13.6	K2	-	1.66	3
TW HyaX47	GSC 7208.0591	stellar-like	71	14.2	K5	0.01 ± 0.05	1.60	3
TW HyaX48	GSC 7208.1111	stellar-like	65	13.6	G1	0.02 ± 0.05	4.63	3
TW HyaX54	GSC 7208.1245	stellar-like	28	15.0	G3	-	3.15	3
TW HyaX56	SAO 202045	stellar-like	21	10.2	G5	0.05 ± 0.05	3.22	1, 3
CoD$-29°8887$X01		cluster [b] (cand.)	-	-				4
CoD$-29°8887$X03	GSC 720100605	pair of galaxies	18	-				2, 3
CoD$-29°8887$X04	GSC 7201.0163	stellar-like	19	12.1	G4	-	2.77	3
CoD$-29°8887$X06		galaxy	-	-				4
CoD$-29°8887$X08	HD 96700	stellar-like	9	6.5	G2	0.02 ± 0.05	3.42	1, 2, 3
CoD$-29°8887$X15	HD 96803	stellar-like	6	7.8	F5	0.03 ± 0.05	5.17	1, 3
CoD$-29°8887$X19	SAO 202139	stellar-like	24	9.9	F6	-	4.86	1, 3
	GSC 7201.0475	stellar-like	22	13.5	K4	-	1.13	3
CoD$-29°8887$X23	**CoD $-$ 29°8887**	stellar-like	4	12.1	M0	0.42 ± 0.10	-2.28	1, 3
CoD$-29°8887$X24	GSC 7201.0551	galaxy	30	15.0				2, 3, 4
	GSC 7201.0289	galaxy	27	15.5				2, 3, 4
CoD$-29°8887$X28		cluster [b] (cand.)	-	-				4
CoD$-29°8887$X29	GSC 7201.0677	stellar-like	12	15.5	G7	-	2.40	3
CoD$-29°8887$X35	GSC 6648.0042	stellar-like	21	11.0	K5	-	1.06	3
CoD$-29°8887$X38	GSC 7201.0853	stellar-like	27	14.3	G0	0.05 ± 0.05	3.55	3
CoD$-29°8887$X40		cluster [b] (cand.)	-	-				4
	HD 97022	stellar-like	86	7.2	K1	-	1.43	1, 3
CoD$-29°8887$X42		galaxy	6	-				4
CoD$-29°8887$X45	HD 97131	stellar-like	19	9.0	F0	0.03 ± 0.05	5.81	1, 3
CoD$-29°8887$X48	Abell 3471	cluster [b]	-	-				2
CoD$-29°8887$X49		cluster [b] (cand.)	-	-				4

[a] object type determined from 1: SIMBAD, 2: NED, 3: GSC, 4: DSS.
[b] means cluster of galaxies

low-mass stars have deep convective layers, lithium is efficiently destroyed and its presence is therefore indicative of the PMS nature of an object.
– A spectral type which is later than F5.
– An Hα line that is filled up by emission or shows pure emission because PMS stars are believed to be chromospherically active.

The K- and M-type stars with Hα in emission but without the LiI absorption line are classified as dKe and dMe stars (Walter et al. 1988). These objects do not belong to the class of PMS stars.

In Table 4, we also summarise the results from our spectroscopic follow-up observations. Column (2) gives the identifier for a counterpart of an X-ray source that has been spectroscopically observed. Column (6) contains the spectral type, and Columns (7) and (8) show the equivalent widths of the LiI $\lambda 6708$ and Hα absorption line, respectively. In case of an emission line the equivalent width is negative.

Only our two main targets (printed boldface) show a high lithium abundance characterising them as young stellar objects. 13 objects show low lithium abundances (EW(LiI) < 0.2Å) mainly being near the detection limit of our mid-resolution spectra. Four objects (TW HyaX04, TW HyaX06, TW HyaX25, TW HyaX39) show an extended chromospheric activity. They are classified as dKe or dMe type stars. To decide from the equivalent width of the LiI absorption line whether the objects are really in a pre-main sequence state, we compared our data to the lithium survey of the Pleiades performed by Soderblom et al. (1993). This comparison shows that indeed only our two main targets are young stellar objects compared to the age of the Pleiades. In these cases the blending with unresolved nearby iron lines should not be a serious problem because for spectral types later than K5 the strength of the iron lines is negligible compared with the lithium lines.

4. Discussion

4.1. X-ray analysis

Our two main objects TW Hya and CoD$-29°8887$ are strong X-ray sources. CoD$-29°8887$ has a X-ray flux comparable to the brightest WTTSs found around nearby star-forming regions. Its hardness ratios $HR1$ and $HR2$ are close to the mean values of the WTTS population, and it shows the expected X-ray to optical flux ratio (Neuhäuser et al. 1995). TW Hya, however, has a ten times brighter X-ray flux than typical CTTSs located in nearby molecular clouds. Its hardness ratios have unusual low values. Especially $HR1 = 0.5$ is nearly a factor of two lower compared to other CTTSs indicating a soft component in the spectrum of TW Hya. These facts could be explained, if we assume only a low amount of absorbing material at the line of sight and a short distance to TW Hya.

From our deep ROSAT observations we gained 3225 photon events for TW Hya and 1765 events related to CoD$-29°8887$. These numbers are sufficient for a detailed analysis of the spectral and temporal behaviour.

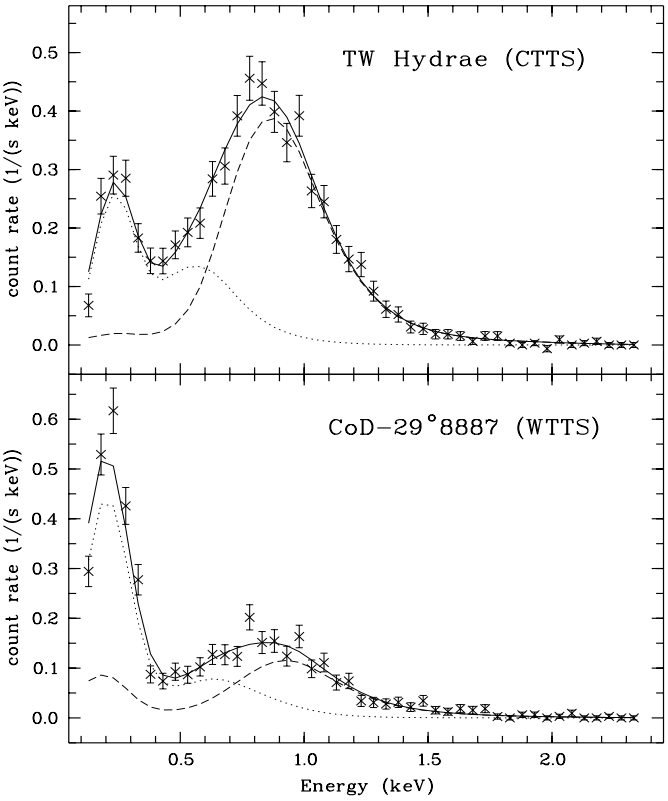

Fig. 2. Observed and fitted model spectra of TW Hya and CoD$-29°8887$

The X-ray emission from TTSs is thought to be produced in an extended solar-like corona, i.e. by an optically thin thermal plasma at high temperatures of $T \sim 10^7$K. An appropriate spectral fit is given by the Raymond-Smith X-ray photon distribution (Raymond & Smith 1977). This model spectrum combines thermal bremsstrahlung emission and absorption lines of heavy elements at high ionisation levels. We used solar abundances for our modelling. The initial approach to fit one-temperature models failed. Therefore, we switched to a two-temperature fit consisting of two Raymond-Smith models. Throughout, we corrected for foreground X-ray absorption by using an absorption law based on Morrison-McCammon atomic cross sections. The plasma models are fitted to the X-ray pulse height distribution using a χ^2-algorithm provided by EXSAS.

In Fig. 2 we show the observed X-ray spectra (crosses with error bars) and the fitted model spectra (solid lines) of TW Hya and CoD$-29°8887$. In each graph we also plotted the low temperature (dotted line) and the high temperature component (dashed line) of the combined fit model. The temperatures of the 'soft' and the 'hard' model components are around $kT_{\rm s} = 0.15$keV ($T_{\rm s} \sim 2 \cdot 10^6$K) and $kT_{\rm h} = 1.0$keV ($T_{\rm h} \sim 10^7$K), respectively. The derived hydrogen column density $N_{\rm H} < 10^{21}/{\rm cm}^2$ indicates that there is nearly no absorbing material along the line of sight towards our two main targets. A detailed list of the fit parameters is given in Table 5.

From the time series analysis of the X-ray data of TW Hya and CoD$-29°8887$ we found evidence for an X-ray variability

Table 5. Parameters from fitting Raymond-Smith models to the X-ray spectra

object name	$N_{\rm H}$ ($10^{21}/cm^2$)	$kT_{\rm s}$ (keV)	$kT_{\rm h}$ (keV)
TW Hya	0.55 ± 0.05	0.14 ± 0.02	0.83 ± 0.08
CoD$-29°8887$	0.13 ± 0.09	0.16 ± 0.47	1.03 ± 0.10

on short time scales (10-100sec), but no single flare could be identified from our data sets.

The X-ray spectrum and the temporal behaviour of the WTTS CoD$-29°8887$ are similar to the ones of nearby solar-like main-sequence stars. This indicates that a solar-like dynamo drives the X-ray emission of CoD$-29°8887$ observed within the energy band of ROSAT. TW Hya is an excellent object to study the X-ray emission of a classical T Tauri star. Since there is nearly no material along the line of sight, we obtain an unbiased X-ray spectrum of TW Hya. It shows that CTTSs really possess stronger X-ray emission at higher energies in comparison with WTTSs (see also the hardness ratios of TW Hya and CoD$-29°8887$ in Tab. 2 and Tab. 3). But this harder X-ray emission cannot result from faster rotation of TW Hya, because its plasma temperatures are lower compared to CoD$-29°8887$ (Güdel et al. 1996).

The low hydrogen column density given in Table 5 for TW Hya proves that there is no material along the line of sight. On the other hand TW Hya is known to be a strong sub-millimetre continuum source (Weintraub et al. 1989). Using a relation provided by Launhardt et al. (1996) we estimated a beam-averaged hydrogen column density $N_{\rm H} = 10^{23}/cm^2$ from the sub-millimetre fluxes. The uncertainty of $N_{\rm H}$ is a factor of 2 to 3. It depends mainly on the uncertainties of the mass absorption coefficient κ (see Ossenkopf & Henning 1994) and to a lesser amount on the dust temperature $T_{\rm d}$. For molecular clouds the value of κ is known within a factor of two and was taken as $0.5{\rm cm}^2/{\rm g}$ at 1.3mm wavelength. The mean dust temperature $T_{\rm d}$ was derived from the 60- and 100-μm IRAS fluxes of TW Hya and is about 35K.

The hydrogen column density we derived from beam averaged sub-millimetre fluxes is about two orders of magnitude higher than the value we derived from our X-ray observation. This indicates that the gas and dust around TW Hya are concentrated in a disk-like configuration seen nearly pole-on. This model for TW Hya is also confirmed by very narrow CO emission lines (Zuckerman et al. 1995, see also Kastner et al. 1997).

We detected TW Hya in the N and Q band by mid-infrared imaging with the MANIAC camera at ESO's 2.2m telescope in June 1997. This detection clearly shows the association of TW Hya with warm dust. The dust emission is slightly extended in north-south direction.

4.2. Distance and space velocities

One way to determine the age of low-mass YSOs is to place them into a HR diagram where the object could be associated with a mass-dependent evolutionary track of a PMS star. For the HR diagram we have to know the bolometric luminosity, effective temperature, and distance of our objects. The distance determined by the Hipparcos satellite of TW Hya is $d = (56 \pm 7)$pc. From photometric observations done by Rucinsky & Krautter (1983) we derived a mean apparent visual magnitude of $m_{\rm V} = 11.25{\rm mag}$ for the variable star TW Hya. Hence, the absolute bolometric magnitude of the K7V star is $M_{\rm bol} = 6.5{\rm mag}$. In the HR-diagram TW Hya is located above the zero-age main sequence (ZAMS). Comparing the location with evolutionary tracks provided by D'Antona & Mazzitelli (1994) we estimate an age of about 10^7 years and a mass of $M = 0.7{\rm M}_\odot$ for TW Hya. Assuming that CoD$-29°8887$ is approximately of the same age as TW Hya, we get $d \approx 45{\rm pc}$ and $M = 0.6{\rm M}_\odot$ for its distance and mass, respectively. Here we used $m_{\rm V} = 11.08{\rm mag}$ from Simbad.

In Table 6 we present space velocities for TW Hya and HD 98800. These are calculated from proper motions and distances from the Hipparcos Main Catalogue and the centre of mass radial velocities from Torres et al. (1995) for HD 98800 and Reipurth et al. (1996) for TW Hya. For the calculation we used an algorithm provided by Johnson & Soderblom (1987) and corrected for the solar space velocity $(U,V,W)_\odot = (+10.3{\rm km/s}, +15.0{\rm km/s}, +7.5{\rm km/s})$ (Boesgaard & Tripicco 1986) relative to the local standard of rest (LSR). The errors of the corrected data are at the same order as the value of the space motion itself. Therefore, we are not able to calculate the precise paths of TW Hya and HD 98800 for the last 10^7 years and it is not excluded that they originate from a common birthplace. At present the mean distance between the objects is about $13{\rm pc}$. This distance could have been travelled at a velocity of about 1km/sec within the past ten million years. TW Hya, CoD$-29°8887$, and HD 98800 may be part of a group of YSOs with low space velocities similar to the subgroups of young stars with mean motions being significantly different from the majority of stars in Taurus-Auriga as found by Jones & Herbig (1979). For such an aggregate of young stars the velocity dispersion is 1-2km/sec which is in good agreement with our calculated space velocities.

The ejection by close encounters of YSOs during the star formation phase is a possible mechanism to isolate young low-mass stars from their parental dark clouds (Sterzik & Durison 1995). In the case of TW Hya, CoD$-29°8887$, and HD 98800 it is very unlikely that this mechanism was operating. HD 98800 is a multiple system of four stars, CoD$-29°8887$ is a visual binary system, and TW Hya is associated with a disk. Specific properties like these would most probably not survive such an ejection process. The space velocities of only some km/sec are also lower than predicted for such models. Hence, we conclude that TW Hya and HD 98800 have not moved far from their original birthplace and the parent dark clouds have been dispersed meanwhile.

Table 6. Space velocities for TW Hya and HD 98800

object name	$\mu_\alpha \cos(\delta)$ (mas/yr)	μ_δ (mas/yr)	π (mas)	$v_{\rm rad}$ (km/s)	U (km/s)	V (km/s)	W (km/s)
TW Hya	-66.90 $\pm$ 1.78	-12.36 $\pm$ 1.42	17.72 $\pm$ 2.21	12 $\pm$ 1	-1.8 $\pm$ 3.3	-2.3 $\pm$ 1.6	2.1 $\pm$ 1.7
HD 98800	-85.45 $\pm$ 1.89	-33.37 $\pm$ 2.12	21.43 $\pm$ 2.12	9.2 $\pm$ 0.7	-2.1 $\pm$ 3.3	-2.8 $\pm$ 2.1	0.4 $\pm$ 3.4

5. Conclusions

The most puzzling aspect of isolated TTSs is the question of their birthplaces. From the kinematics of TW Hya and HD 98800, we infer that they have formed close to their present positions. From the age of about 10^7 yrs and the low space velocities of 3-4km/sec derived in this paper, we conclude that they have not travelled far away from their places of origin.

Our sophisticated X-ray detection procedure revealed altogether 107 sources. Among these there are 37 stellar-like objects brighter than $m_{\rm V} = 16$mag. A careful discussion based on our spectroscopic follow-up observations showed only two of them, namely our main targets TW Hya and CoD-29°8887, to be TTSs. This clearly demonstrates that the latter objects were not born at their present positions together with other stars brighter than $m_{\rm V} = 16$mag and being closer to each other than about $57'$. In case of a presumed star-forming region as close as 50pc this low surface density is not unexpected. For typical low-mass star-forming region as Taurus-Auriga (distance 140pc), Wichmann et al. (1996) give median nearest-neighbour distances of $8.1'$ and $41'$ for the star-forming core of the region and the outer field of WTTSs, respectively. For our region this scales to 1° and 5°, respectively. These numbers will decrease by less than a factor of 1.5 if the fainter limiting X-ray luminosity reached in our data is taken into account. This is because Wichmann et al. (1996) sampled already 60% of previously unknown WTTS in the Taurus-Auriga star-forming region.

The group of isolated TTSs around TW Hya are the closest known low-mass young stellar objects. They provide the excellent possibility to study young solar-like stars at a distance of about $d \approx 50$pc, three times closer than the objects in nearby star-forming regions like the Taurus-Auriga complex or the Chamaeleon clouds. The presence of circumstellar disks around TW Hya and HD 98800 offers the chance for detailed investigations of such structures with high spatial resolution.

Acknowledgements. This research was supported by BMBF Verbundforschung under grants 05 2JN12A and 05 JN12A. We thank J. M. Alcalá (Naples) and M. Braun (Villafranca) for valuable discussions during the course of this work.

References

Boesgaard A.M., Tripicco M.J. 1986, ApJ, 303, 724
D'Antona F., Mazzitelli I. 1994, ApJS, 90, 467
de la Reza R., Torres C.A.O., Quast G., Castilho B.V., Vieira G.L. 1989, ApJ, 343, L61
Feigelson E.D.,1987, Protostars and molecular clouds. Montemerle Th. and Bertout C. (eds.). CEN Saclay, Gif-sur-Yvette, 123
Feigelson E.D., 1996, ApJ 468, 306
Gregorio-Hetem J., Lépine J.R.D., Quast G., Torres C.A.O., de la Reza R. 1992, AJ, 103, 549
Grinin V.P., Kiselev N.N., Minikulov N.Kh. et al. 1991, ApJS, 186, 283
Güdel M., Guinan E.F., Skinner S.L. 1996, Röntgenstrahlung from the Universe. Zimmermann H.U., Trümper J.E., Yorke H. (eds.), MPE Report 263, 39
Henize K.G. 1976, ApJS, 30, 491
Hoffmeister C. 1943, Kleinere Veröff. Berlin-Babelsberg, No. 27
Johnson D.R.H., Soderblom D.R. 1987, AJ, 93, 864
Jones B.F., Herbig G.H. 1979, AJ, 84, 1872
Kastner J.H., Zuckerman B., Weintraub D.A., Forveille T. 1997, Sci, 277, 67
Launhardt R., Mezger P.G., Haslam C.T.G., Kreysa E., Lemke R., Sievers A., Zylka R. 1996, A&A, 312, 569
Launhardt R., Henning Th. 1997, in preparation
Neuhäuser R., Sterzik M.F., Schmitt J.H.M.M., Wichmann R., Krautter J. 1995, A&A, 297, 391
Neuhäuser R. 1997 Science 176, 1363
Ossenkopf V., Henning Th. 1994 A&A, 291, 943
Palla F., Galli D. 1997, ApJ, 476, L35
Pfau, W., Hoff W., Relke H. 1998, in preparation
Raymond J.C., Smith B.W., 1977, ApJS, 35, 419
Reipurth B., Pedrosa A., Lago M.T.V.T. 1996, A&AS, 120, 229
Rucinski S.M., Krautter J. 1983, A&A, 121, 217
Sandqvist, Aa. 1977, A&A 57, 467
Soderblom D.R., Jones B.F., Balachandran S., Stauffer J.R., Duncan D.K., Fedele S.B., Hudon J.D. 1993, AJ, 106, 1095
Soderblom D.R., Henry T.J., Shetrone M.D., Jones B.F., Saar S.H. 1996, ApJ, 460, 984
Sterzik M., Durisen R. 1995, A&A, 304, L9
Thé, P.S., de Winter, D., Pérez, M.R. 1994, A&AS, 104, 315
Torres, G., Stefanik, R.P., Latham, D.W., Mazeh 1995, ApJ, 452, 870
Trümper J., et al. 1991, Nat, 349, 579
Walter F.M., Brown A., Mathieu R.D., Myers P.C., Vrba F.J. 1988, AJ, 96, 297
Weintraub D.A., Sandell G., Duncan W.D. 1989, ApJ, 340, L69
Wichmann, R., Krautter, J., Schmitt, J.H.M.M., Neuhäuser, R., Alcalá, J.M., Zinnecker, H., Wagner, R.M., Mundt, R., Sterzik, M.F. 1996, A&A 312, 439
Zuckerman B., Becklin E.E. 1993, ApJ, 406, L25
Zuckerman B., Forveille T., Kastner J.H. 1995, Nat, 373, 494